

Unique Chirality Selection in Neural Cells for D-Matrix Enabling Specific Manipulation of Cell Behaviors

Yi Li, Yulin Wang, Qiang Ao, Xiaohui Li, Zhongbing Huang,* Xiaoqiu Dou, Ning Mu, Ximing Pu, Juan Wang, Tunan Chen, Guangfu Yin, Hua Feng, and Chuanliang Feng*

Manipulating neural cell behaviors is a critical issue to various therapies for neurological diseases and damages, where matrix chirality has long been overlooked despite the proven adhesion and proliferation improvement of multiple non-neural cells by L-matrixes. Here, it is reported that the D-matrix chirality specifically enhances cell density, viability, proliferation, and survival in four different types of neural cells, contrasting its inhibition in non-neural cells. This universal impact on neural cells is defined as “chirality selection for D-matrix” and is achieved through the activation of JNK and p38/MAPK signaling pathways by the cellular tension relaxation resulting from the weak interaction between D-matrix and cytoskeleton proteins, particularly actin. Also, D-matrix promotes sciatic nerve repair effectively, both with or without non-neural stem cell implantation, by improving the population, function, and myelination of autologous Schwann cells. D-matrix chirality, as a simple, safe, and effective microenvironment cue to specifically and universally manipulate neural cell behaviors, holds extensive application potential in addressing neurological issues such as nerve regeneration, neurodegenerative disease treatment, neural tumor targeting, and neurodevelopment.

1. Introduction

Manipulating neural cell behaviors, especially improving proliferation and survival, is essential in various therapies for

neurological diseases and damages.^[1] One promising approach is the construction of a functional artificial extracellular matrix designed to provide mechanical and biochemical cues.^[2] However, current methods only offer partial regulation of neural cell behaviors by modulating the matrix composition, stiffness, topology, and conductivity, which do not fully capture the complex ultrastructure and functionality of the natural extracellular matrix in mammals.^[2,3] Chirality, an intrinsic property found at multiple levels of organisms, from molecule structures to left-right body asymmetry,^[4] has long been overlooked in the design of artificial neural matrixes despite the demonstrated influences on immune response and stem cell fate,^[5] because of the insufficient attention toward matrix chirality in research on microenvironmental cues impacting neural cells.

Therefore, investigating the impact of matrix chirality on neural cells through constructing a chiral microenvironment is

a critical scientific endeavor. One simple method involves fabricating a surface consisting of chiral molecules, which has been reported to effectively alter the material targeting to amyloid aggregates and influence cell adhesion on matrixes.^[6] To regulate cell fates and behaviors,^[5c-e,7] developing intensive 3D microenvironments with chiral symmetry using chiral supramolecular hydrogels self-assembled from peptide derivatives provides a more ideal solution.^[5c,7c,8] Numerous studies involving various non-neural cells have consistently shown that cell viability, proliferation, and adhesion are improved by the L-chirality of different matrixes.^[6b-f,7a,c] However, neural cells appear to exhibit different responses, where neuronal growth degenerates upon exposure to the L-cysteine enantiomer and neuronal differentiation of retinal progenitor cells is promoted by the D-matrix.^[9] These contrasting results not only generate uncertainty regarding the applicability of matrix chirality in the nervous system but also suggest the possibility of a specific impact of D-matrixes on neural cells. To better understand the impact and furnish an application foundation for matrix chirality as a microenvironmental cue in manipulating neural cell behaviors, further investigation into the neural cell response to matrix chirality is crucially required.

Herein, we have confirmed the universality and specificity of D-matrix selection in neural cells. Our results show that the D-chirality of supramolecular hydrogel enhances cell viability,

Y. Li, Y. Wang, Q. Ao, X. Li, Z. Huang, X. Pu, J. Wang, G. Yin
College of Biomedical Engineering

Sichuan University
Chengdu 610065, China
E-mail: zhuang@scu.edu.cn

X. Dou, C. Feng
State Key Lab of Metal Matrix Composites
School of Materials Science and Engineering
Shanghai Jiao Tong University
Shanghai 200240, China
E-mail: clfeng@sjtu.edu.cn

N. Mu, T. Chen, H. Feng
Third Military Medical University Southwest Hospital
Chongqing 400038, China

Y. Li, Y. Wang, Q. Ao
Institute of Regulatory Science for Medical Devices
Sichuan University
Chengdu 610065, China

 The ORCID identification number(s) for the author(s) of this article can be found under <https://doi.org/10.1002/adma.202301435>

DOI: 10.1002/adma.202301435

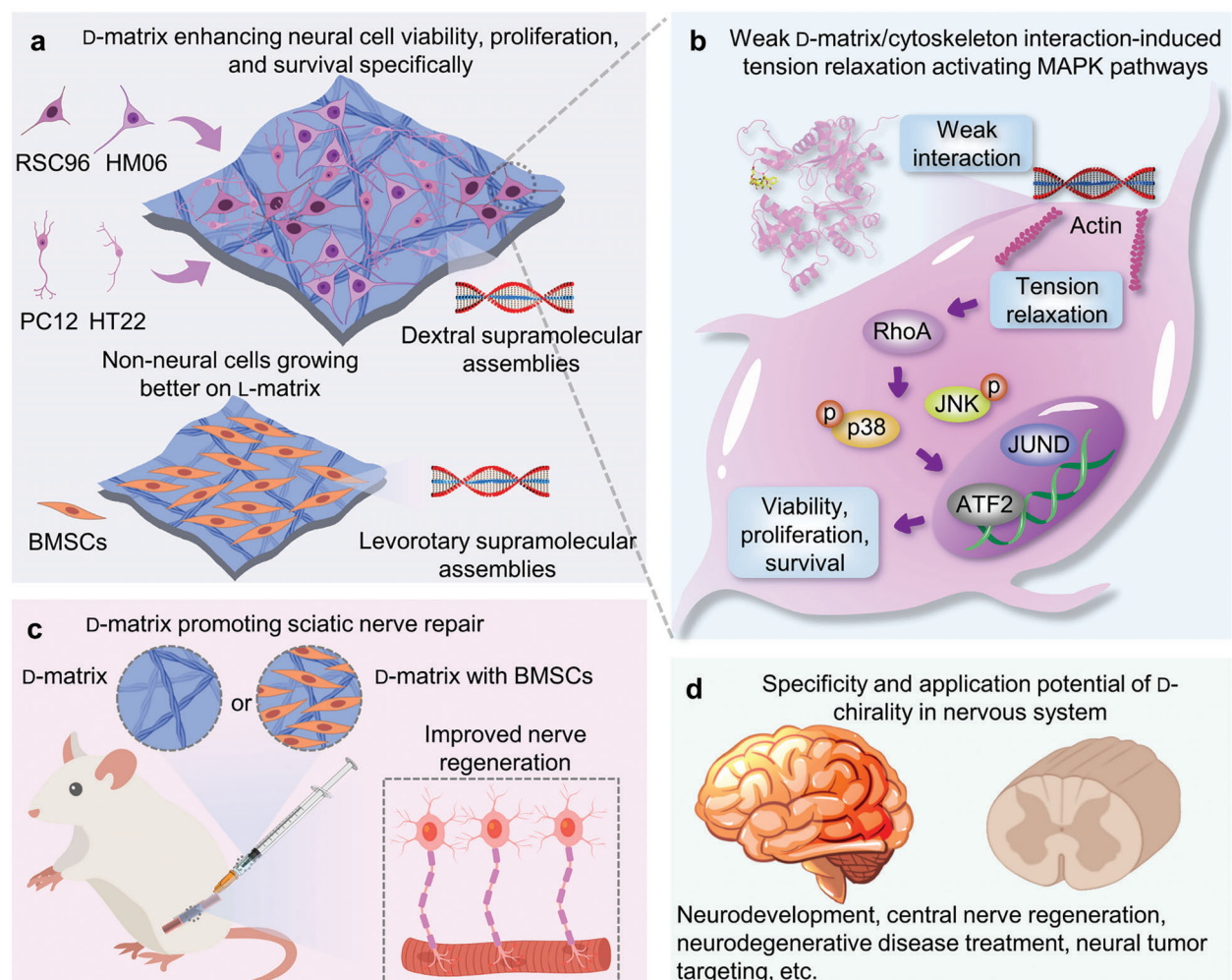


Figure 1. Specific manipulation of neural cells by D-matrix chirality. a) Schematic illustration depicting D-matrix enhancing the viability, proliferation, and survival of four types of neural cells, while L-matrix promotes the growth of non-neural cells. b) Schematic illustration depicting the molecular mechanism that cellular tension relaxation resulting from the weak interaction between D-matrix and cytoskeleton activates JNK and p38/MAPK signaling pathways. c) Schematic illustration depicting the effective promotion of sciatic nerve repair by injected D-matrix with or without BMSCs implantation. d) Neurological issues where D-chirality has potential specificity and applications.

proliferation, and survival of four different types of neural cells, in contrast to the universal L-matrix selection observed in non-neural cells (**Figure 1a**). The molecular mechanism was investigated, showing that weaker interaction between D-matrix and cytoskeleton results in cellular tension relaxation, subsequently leading to the activation of JNK and p38/MAPK signaling pathways (**Figure 1b**). Notably, D-matrix chirality comprehensively promotes sciatic nerve repair in two treatment strategies (**Figure 1c**). These findings indicate that D-matrix chirality is a simple and effective physicochemical cue specifically and universally manipulating neural cell behaviors in the establishment of various material systems for nervous system issues (**Figure 1d**).

2. Results and Discussion

2.1. Construction of Chiral Hydrogel Matrixes

First, phenylalanine derivative enantiomers (D-ph and L-ph) were synthesized (Figures S1 and S2, Supporting Information) to self-

assemble into chiral supramolecular hydrogels (**Figure 2a**), considering the acceptable biocompatibility. As shown in Figure 2b,c, the resulting D-ph hydrogel (DH) and L-ph hydrogel (LH) exhibited well-defined mirror-symmetrical chirality in their self-assembly structures, as evidenced by circular dichroism (CD) signals of equal intensity but opposite chirality. The enhanced spectral peaks of hydrogels shifted to 230 and 270 nm from 218 and 237 nm of the enantiomer solutions,^[10] which were attributed to the amide carbonyl group and phenyl group,^[11] respectively. And racemic hydrogels (RH), formed by mixing D-ph and L-ph at a 1:1 molar ratio, displayed no CD signals. Microscopic analysis (Figure 2d,e; Figure S3a, Supporting Information) revealed that both DH and LH consisted of helical nanofibers with average diameters of 64.3 ± 13.5 nm and helical pitches of 521.3 ± 163.4 nm, but opposite helical directions, while RH was composed of non-helical nanofibers with a slightly larger average diameter (116.9 ± 23.1 nm) due to weaker regularity. Furthermore, all three hydrogels exhibited comparable stiffness with a storage modulus G' of ≈ 2.2 kPa and a loss modulus G''

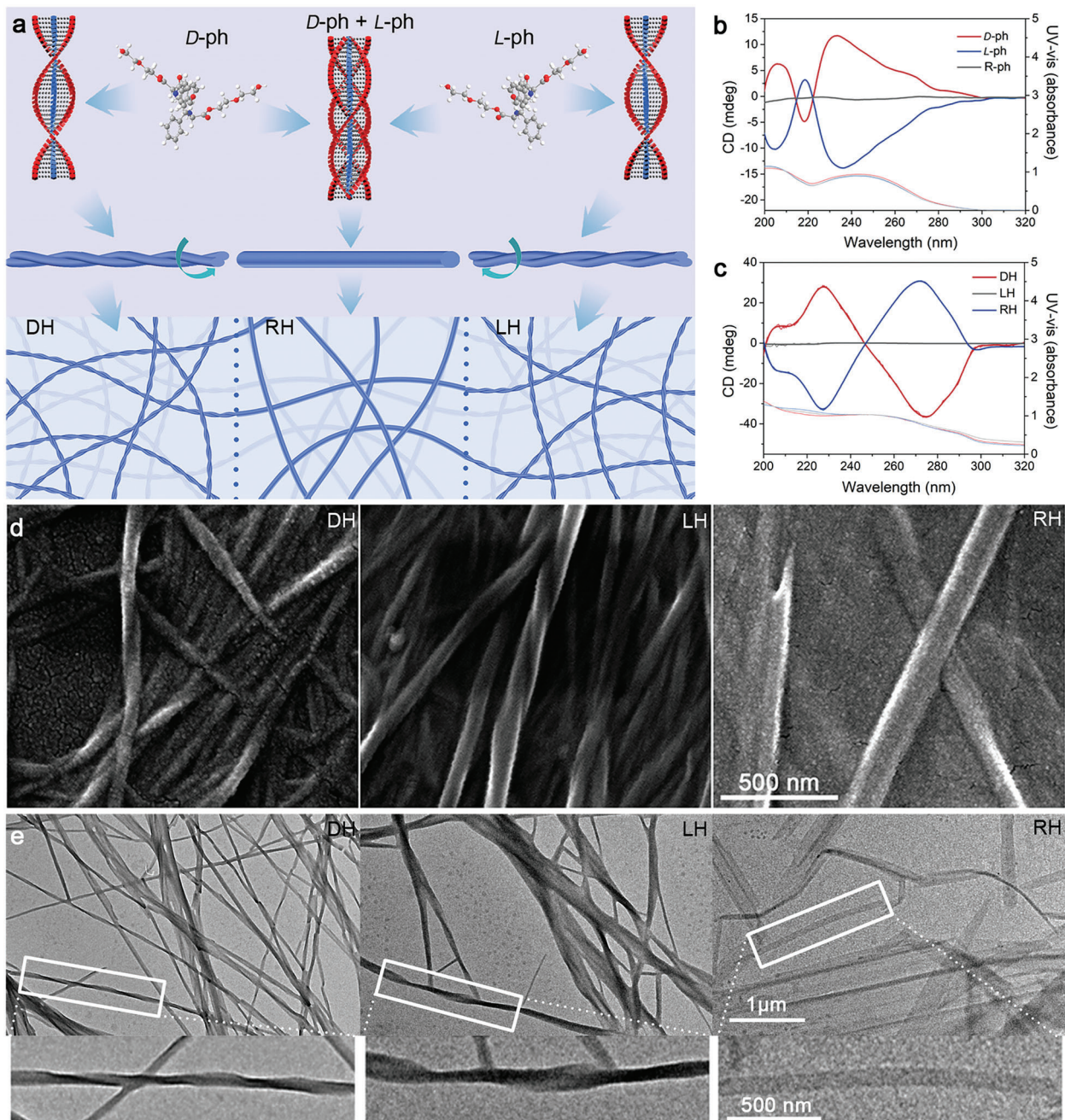


Figure 2. Preparation and characterization of chiral matrixes. a) Schematic representation illustrating chiral matrix fabrication through self-assembly. b,c) CD spectra (in dark colors) and corresponding UV-vis spectra (in light colors) of D-ph, L-ph, and R-ph monomers and DH, LH, and RH assemblies. d,e) Representative helix morphology of the chiral matrix nanofibers under SEM and TEM.

of 0.6 kPa (Figure S3b, Supporting Information). These results suggested that the three hydrogels possessed similar properties, with mirror-symmetrical chirality being the only variable.

2.2. Effect of Matrix Chirality on Neural Cell Behaviors

To investigate the effect of chirality on various cell behaviors, different neural cell lines were cultured on the three hydrogel ma-

trices. Specifically, RSC96 cells (rat Schwann cell line), HM06 cells (human microglial cell line), PC12 cells (neuron-like cell line), and HT22 cells (mouse hippocampal neuron cell line) were chosen due to their extensive use in neurological research involving both peripheral and central nerves as crucial glial cells and neurons.^[12] Initially, the overall cell viability was assessed using Live/Dead staining and Cell Counting Kit-8 (CCK-8) assays, and all four types of cells had the highest cell density and viability on the DH matrix and the lowest on the LH matrix, significantly

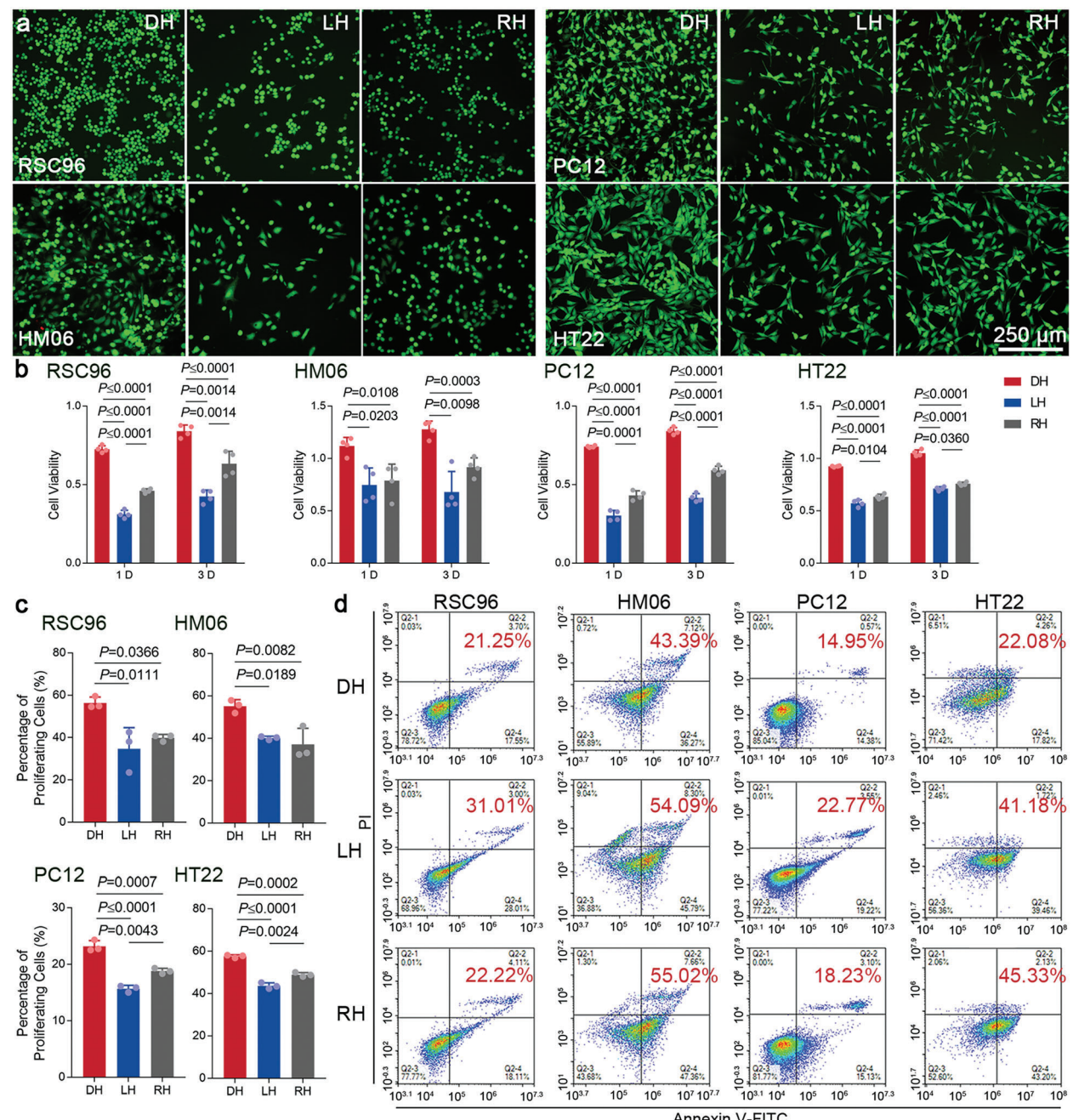


Figure 3. Impact of matrix chirality on neural cell behaviors. a) Representative fluorescence microscopy images of the four types of neural cells cultured on the three chiral matrixes for 3 days and processed with Live (green) and Dead (red) staining. b) Cell viabilities of the four types of neural cells on the three chiral matrixes through CCK-8 assays. c) Quantitative analysis of the proliferating cell percentage among the four types of neural cells cultured on the three chiral matrixes, based on the results of EdU test. d) Representative percentage of apoptotic neural cells (indicated by red numbers, representing the sum of the second and fourth quadrants) determined by flow cytometric analysis with Annexin V-FITC/PI staining. Values in (b) and (c) represent the mean ± s.d. ($n = 4$ for b) and $n = 3$ for c). Statistical significance and P values were determined by one-way analysis of variance (ANOVA) followed by Tukey's multiple comparison test.

(Figure 3a,b; Figure S4, Supporting Information). Subsequently, the proliferation and apoptosis of cells, crucial factors determining cell population, were investigated with 5-ethynyl-2'-deoxyuridine (EdU) Image Kit and an Annexin V-fluorescein isothiocyanate/propidium iodide (Annexin V-FITC/PI) Apoptosis Detection Kit, respectively. Each DH group of the four types

of neural cells exhibited the largest numbers of EdU-positive proliferating cells (Figure S5, Supporting Information) and the significantly highest proliferation rates (Figure 3c). Meanwhile, the apoptosis rates in DH groups were the lowest (Figure 3d), indicating the best survival. These results suggest that the D-matrix chirality promotes cell density, viability, proliferation, and

survival in the four types of neural cells, compared to the L-chirality and commonly used achirality. Additionally, the viability of neural cells cultured in matrix extract medium did not consistently exhibit significant differences among the three groups (Figure S6a, Supporting Information). However, on non-assembled gelator layers, the DH group showed slightly higher viability than the LH group only at 1 D (Figure S6b, Supporting Information). These results indicate that the chirality impact on neural cells is induced by the matrix itself rather than dissolved gelators, and the self-assembly of the hydrogels amplifies this impact. Therefore, we define this phenomenon as “chirality selection for the D-matrix” in the four types of neural cells.

2.3. Different Matrix Chirality Selection between Neural Cells and Non-Neural Cells

The chirality-induced cell adhesion difference is the mainstream explanation for the L-matrix selection in non-neural cells.^[5f,6b,d,7a,b] Here, the expression of three proteins in focal adhesion complexes of RSC96 cells was examined using immunofluorescence (IF) staining and western blot (WB) assays. Surprisingly, no significant adhesion difference was observed among the groups (Figure S7, Supporting Information). For comparison, bone marrow stromal cells (BMSCs), as a non-neural cell extensively used in neurological strategies, were selected to confirm the L-matrix selection on the prepared chiral supramolecular hydrogels and showed the highest cell density (Figure S8a, Supporting Information), viability (Figure S8b, Supporting Information), and the lowest apoptosis rate (Figure S8c, Supporting Information) in the LH group. Whereas the cell-matrix adhesion was also improved, as evidenced by the significantly increased expression of adhesion proteins (Figure S9, Supporting Information), which was consistent with previous reports on the L-matrix selection in other non-neural cells.^[6e,f,7a,c] These contrasting chirality effects on cell-matrix adhesion imply a mechanism different from cell adhesion responsible for D-matrix selection in neural cells.

The differential adsorption of serum proteins on chiral matrixes has been reported as another potential factor contributing to the L-matrix selection of non-neural cells.^[5f,6b,d,7a,b] Here, these four types of neural cells and BMSCs were cultured in medium with gradient-content serum, and their viability was examined using CCK-8 assays (Figure S10a–d, Supporting Information). To visualize and quantify the effect of matrix chirality on cells, a chirality impact factor was defined as the rate of the difference in cell viability between chiral and corresponding achiral matrixes to the cell viability on the achiral matrix: chirality impact factor = $(\text{Viability}_{\text{chiral-matrix}} - \text{Viability}_{\text{achiral-matrix}}) / \text{Viability}_{\text{achiral-matrix}}$. A positive value indicates a positive effect, while a negative value indicates a negative effect, and the absolute value represents the strength of the impact. As shown in Figure 4a and Figure S10e (Supporting Information), the chirality impact factor of D-matrix decreased as the serum percentage increased, suggesting the strongest D-matrix effect on neural cells in serum-free culture and a progressive inhibition of D-chirality selection in neural cells due to the serum protein adsorption on matrixes. In contrast, the value of the chirality impact factor on BMSCs increased from a value close to zero as the serum content increased

(Figure S10f,g, Supporting Information), suggesting that matrix chirality selection of BMSCs was indirectly induced by serum protein adsorption on the matrixes. These results further demonstrate that matrix chirality selection of neural cells is achieved through the direct effect of chirality on cellular proteins and is attenuated by the adsorption of serum proteins on matrixes, which is opposite to non-neural cells.

2.4. Weak Interaction between D-Matrix and Neural Cytoskeleton

To investigate the chirality effect of matrixes on the interaction with cellular proteins, serum proteins were employed as a readily available protein kit that closely resembles cellular proteins. After the three chiral gels were soaked in medium with 20% serum for 6 h to reach equilibrium, the amounts of adsorbed proteins showed no significant difference (Figure S11a, Supporting Information), indicating that there was no overall difference in protein adsorption among the chiral matrixes. To obtain detailed information on the chirality-induced difference in matrix affinity with specific proteins, comparative proteomics analyses of adsorbed serum proteins were performed. Over 500 proteins were identified in each group (Figure S11b, Supporting Information), and multiple proteins showed chirality-induced adsorption differences, especially between the DH and LH groups (Figure S11c, Supporting Information). Gene Ontology (GO) enrichment analyses of these differential proteins were performed to clarify the involved biological processes (BP), molecular functions (MF), and cellular components (CC). As shown in Figure 4b, extensive neurologically relevant BP and CC terms were enriched in the analyses of downregulated proteins of the DH group compared to the LH group (involved proteins are listed in Table S1, Supporting Information) and the RH group (listed in Table S2, Supporting Information), suggesting that massive proteins with the weakest adsorption on the DH matrix were relevant to the nervous system. With functions and descriptions of these proteins summarized in Table S3 (Supporting Information), five of these proteins were related to the cytoskeleton, among which actin was the fundamental protein forming the cytoskeleton and was involved in each neurologically relevant term (marked in bold), indicating that the attenuated matrix interaction with the neural cell cytoskeleton, especially actin, by D-chirality might play a critical role.

The reduced amount of actin adsorption on the D-matrix, as evidenced by the WB assay (Figure 4c), further substantiated the weaker interaction between actin and the D-matrix. To investigate the enantioselectivity mechanism between actin and chiral matrixes, molecular dynamics (MD) simulation was implemented. As shown in Figure 4d, D-ph experienced displacement relative to actin and migrated to the adjacent binding pocket during the simulation, while the position of L-ph remained relatively stable with no considerable shift. Molecular mechanics-generalized born surface area (MM-GBSA) analysis (Figure 4e) demonstrated that van der Waals interactions played a primary role in the binding energy, and the D-ph-actin complex, with lower van der Waals energy, exhibited a weaker interaction. The interaction analysis (Figure S11d, Supporting Information) also revealed that D-ph formed relatively fewer hydrogen bonds and other interactions than L-ph. The significant fluctuation and

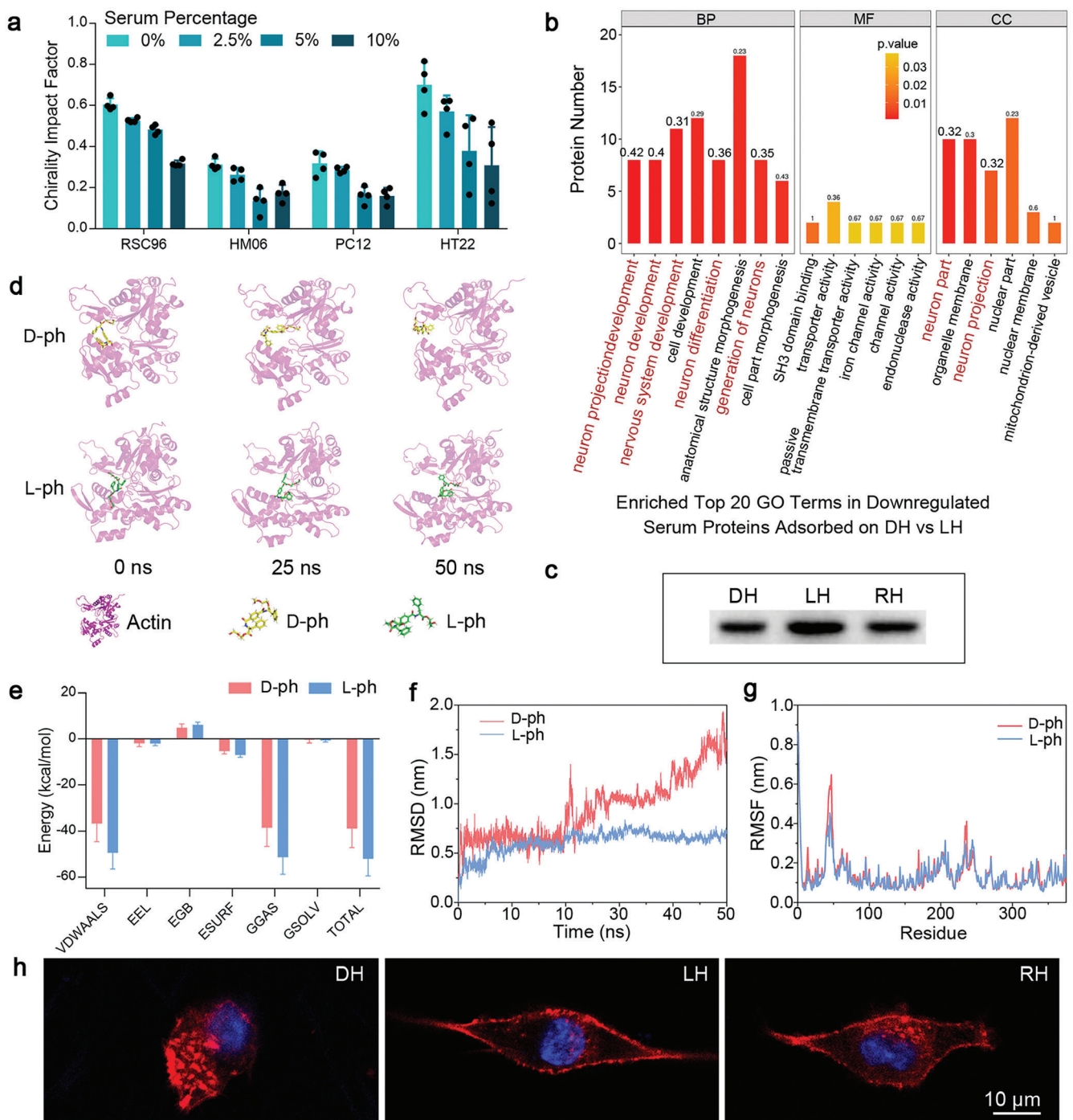


Figure 4. Interaction difference between cytoskeleton and different chiral matrixes. a) Chirality impact factor of D-matrix on neural cells cultured in medium with varying serum content. b) Top 20 enriched GO terms in downregulated serum proteins adsorbed on DH matrix compared with LH group. The marked numbers represent rich factors, and BP, MF, and CC are abbreviations for biological process, molecule function, and cellular component, respectively. c) Representative images of actin adsorption on chiral matrixes by WB assays. d) Snapshots of MD simulation illustrating the effect of chirality on actin interaction. e) Computed binding free energy of the interaction between D/L-ph and actin using MM-GBSA method based on MD simulation. f) RMSD value depicting the bind stability between D/L-ph and actin based on MD simulation. g) RMSF value depicting the structural adaptability of actin residues binding with D/L-ph based on MD simulation. h) Representative images of phalloidin-stained actin (red) in RSC96 cells cultured on chiral matrixes. DAPI-stained nuclei are shown in blue. Values in (a) represent the mean \pm s.d. ($n = 4$). P values in (b) were determined by Fisher's exact test followed by Benjamin-Hochberg correction.

overall upward trend of the root mean square deviation (RMSD) in the D-ph curve (Figure 4f) further demonstrated the lower stability of the D-ph-actin complex. And the higher value of the root mean square fluctuation (RMSF) of the D-ph-actin complex (Figure 4g) indicated the weaker adaptability of each amino acid residue. Overall, these MD simulation results suggest that the chirality influences the binding mode between gelators and actin, and the interaction between D-ph and actin is considerably weaker compared to L-ph. Furthermore, the cytoskeleton staining of RSC96 cells (Figure 4h) showed that cells in the DH group exhibited a contractive morphology with indistinct cellular poles, while cells in the LH and RH groups exhibited a stretched morphology with considerably distant poles, indicating the relaxed cellular tension by the D-matrix. These results suggest that the D-chirality attenuates the interaction between matrix and cytoskeleton-associated proteins, particularly actin, resulting in cell contraction and tension relaxation.^[13]

2.5. MAPK Pathway Activation in RSC96 Cells by D-Matrix Chirality

To explore the intracellular response to matrix chirality, the proteomes of RSC96 cells cultured on the three matrixes were identified and processed with Kyoto Encyclopedia of Genes and Genomes (KEGG) pathway enrichment analyses. Among the upregulated pathways in the DH group compared to both LH and RH groups (Figure 5a; Figure S12a, Supporting Information), most of the enriched pathways were related to metabolism and immunity (Table S4, Supporting Information). Notably, the mitogen-activated protein kinases (MAPK) pathway was the only one regulating cellular functions, including proliferation, differentiation, survival, aging, and death, which is also known to mediate intracellular responses to extracellular matrix signals.^[14] Therefore, the activation of the MAPK pathway was considered the most probable intracellular mechanism by which neural cells respond to matrix chirality stimuli and subsequently alter cell behaviors accordingly. The MAPK components in RSC96 cells cultured on chiral matrixes were examined by WB assays with antibodies against extracellular signal-regulated kinase (ERK), c-Jun N-terminal kinase (JNK), and p38 mitogen-activated protein kinases (p38), as well as their phosphorylated forms (p-ERK, p-JNK, and p-p38). As shown in Figure 5b, the p-JNK and p-p38 proteins in the DH group were significantly upregulated, while the ERK and p-ERK proteins showed no variation, suggesting that two MAPK subfamilies, JNKs and p38s, were activated in RSC96 cells due to D-chirality. Considering the initial effect of matrix chirality on inducing tension relaxation of the cytoskeleton, the cytoskeleton regulation switch, Ras homolog family member A (RhoA),^[15] in the MAPK pathway, might be the crucial upstream protein. The KEGG analysis-enriched MAPK pathway proteins were listed in Table S5 (Supporting Information), and the positive regulation proteins of cell growth and anti-apoptosis, transcription factor JUND and activating transcription factor 2 (ATF-2), in the downstream of JNK and p38 subfamilies were considered pivotal. The upregulated expression of RhoA, JUND, and ATF2 in the DH group at both protein (Figure 5b) and gene (Figure 5c) levels further substantiated the activation of JNK and p38/MAPK pathways by D-matrix.

After silencing RhoA through siRNA transfection, the gene expression of JUND and ATF2 decreased by approximately tenfold in DH group and only two to threefold in the RH group, while the expression level remained unchanged in the LH group (Figure 5d). And the phosphorylation of JNK and p38 in the DH group was blocked in all groups (Figure 5e). These results demonstrate that RhoA is the crucial protein mediating the activation of JNK and p38/MAPK pathways in response to D-matrix-induced relaxation of the cytoskeleton. When JNK and p38 were directly inhibited using SP 600 125 and SB 203 580 inhibitors, respectively, the chirality impact factor of D-matrix decreased significantly to an approximate value of zero (Figure 5f; Figure S12b, Supporting Information), indicating that the achievement of D-matrix selection in neural cells required the simultaneous activation of both JNK and p38 MAPK pathways. Moreover, the equal low expression of ATF2 among the three groups after the inhibition of either JNK or p38 (Figure 5g) suggested that the upregulation of ATF2 required the collaboration of both JNK and p38 pathways. In contrast, the upregulated expression of JUND was only inhibited by the co-inhibition of both JNK and p38, indicating that both pathways separately upregulated JUND expression.

2.6. Mechanism of Chirality Selection for D-matrix in Neural Cells

Based on these results above, a molecular mechanism for the specific manipulation of neural cells by D-matrix chirality is proposed (Figure 5h). The chirality recognition^[16] alters the interaction orientation between matrix molecules and cytoskeletal proteins, especially actin (Figures 5h(i) and 4b–d; Tables S1–S3, Supporting Information). The hydrogen bonds and van der Waals forces between D-matrix and cytoskeletal proteins are reduced significantly (Figure 4e–g; Figure S11d, Supporting Information), resulting in weaker constraint force and morphological contraction on neural cells (Figures 5h(ii) and 4h). This cellular tension relaxation, resulting from the weak interaction between D-matrix and cytoskeleton, activates the JNK and p38/MAPK pathways (Figure 5h(iv) and 5a–c; Figure S12a, Supporting Information) through RhoA (Figure 5h(iii) and 5d,e). Subsequently, the expression of transcription factors JUND and ATF2 is upregulated (Figure 5h(v) and 5b,c,g), ultimately enhancing the viability, proliferation, and survival of neural cells (Figures 5h(vi), 5f, and 3).

2.7. D-Matrix Chirality Promoting Peripheral Nerve Repair

Considering the crucial role of Schwann cells in peripheral nerve regeneration, D-chirality is potentially efficacious in peripheral nerve repair. Before application, the expression of three proteins involved in neurological functions was additionally evaluated using IF staining, which were the markers of glial cell injury or activation, glial fibrillary acidic protein (GFAP) and S100,^[17] as well as the regulator of differentiation and apoptosis, p75 neurotrophin receptor (p75^{NTR}).^[18] The significantly highest fluorescence intensities of the three proteins in the DH group (Figure 6a) indicated the enhancement of activation and redifferentiation of Schwann cells by D-matrix chirality, further substantiating the

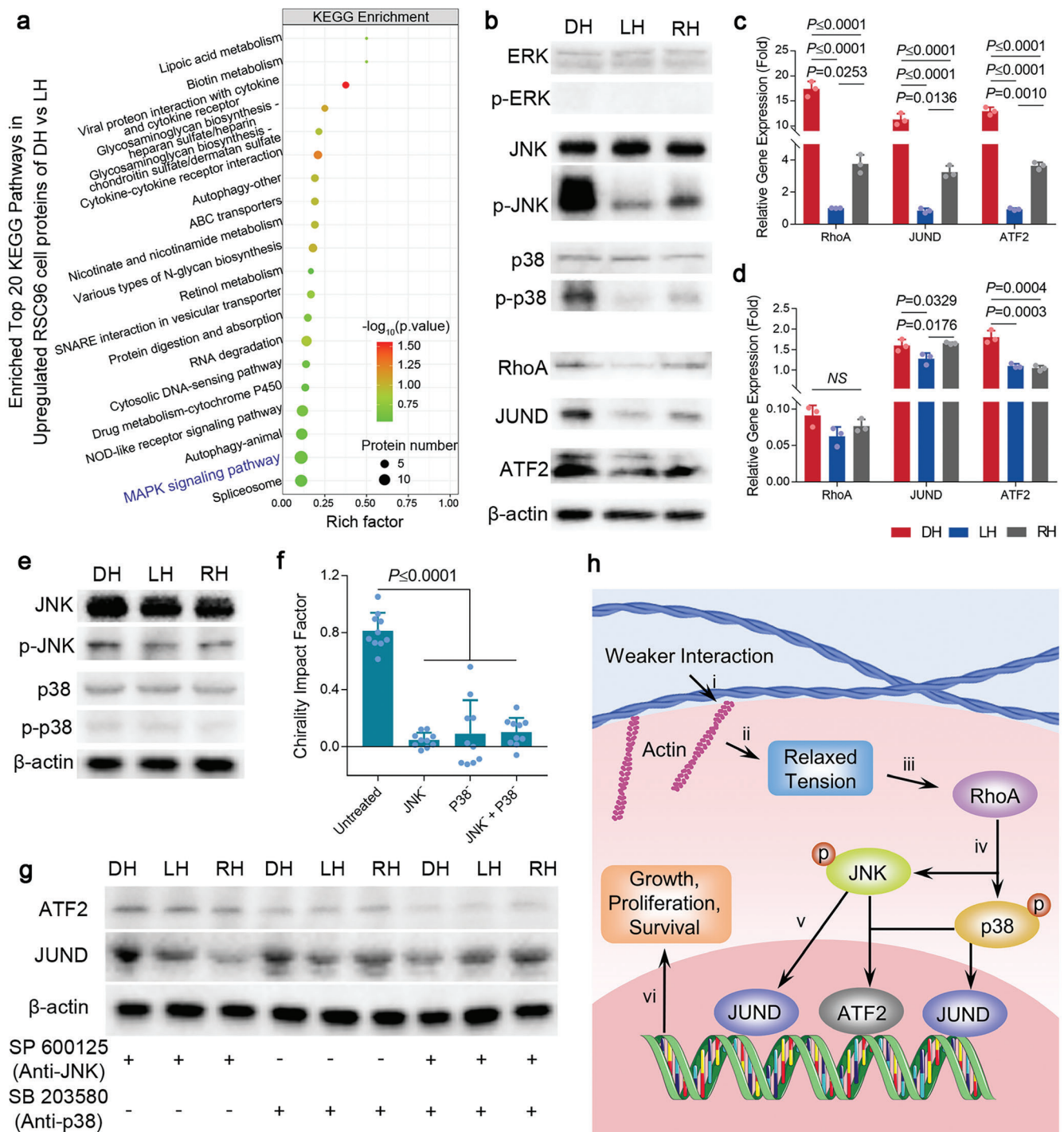


Figure 5. Activation of MAPK pathway in RSC96 cells by D-chirality. **a)** Top 20 enriched KEGG pathways in upregulated proteins of RSC96 cells cultured on D-matrix compared to L-matrix. **b)** Representative expressions of MAPK pathway proteins by WB assays. **c,d)** Relative gene expressions of MAPK pathway proteins by RT-qPCR in regular culture and after RhoA silencing with siRNA. **e)** WB assay images presenting phosphorylation of JNK and p38 after RhoA silencing. **f,g)** Chirality impact factor of D-matrix on RSC96 cells and representative expressions of downstream ATF2 and JUND proteins by WB assays under treatment with JNK and p38 inhibitors. **h)** Schematic representation of molecular mechanism in RSC96 cells manipulated by D-matrix. Values in (c), (d), and (f) represent the mean \pm s.d. ($n = 3$ for (c) and (d)), and $n = 10$ for (f)). P values in a were determined by Fisher's exact test followed by Benjamin-Hochberg correction. Statistical significance and P values in (c, d, and f) were determined by one-way ANOVA followed by Tukey's multiple comparison test.

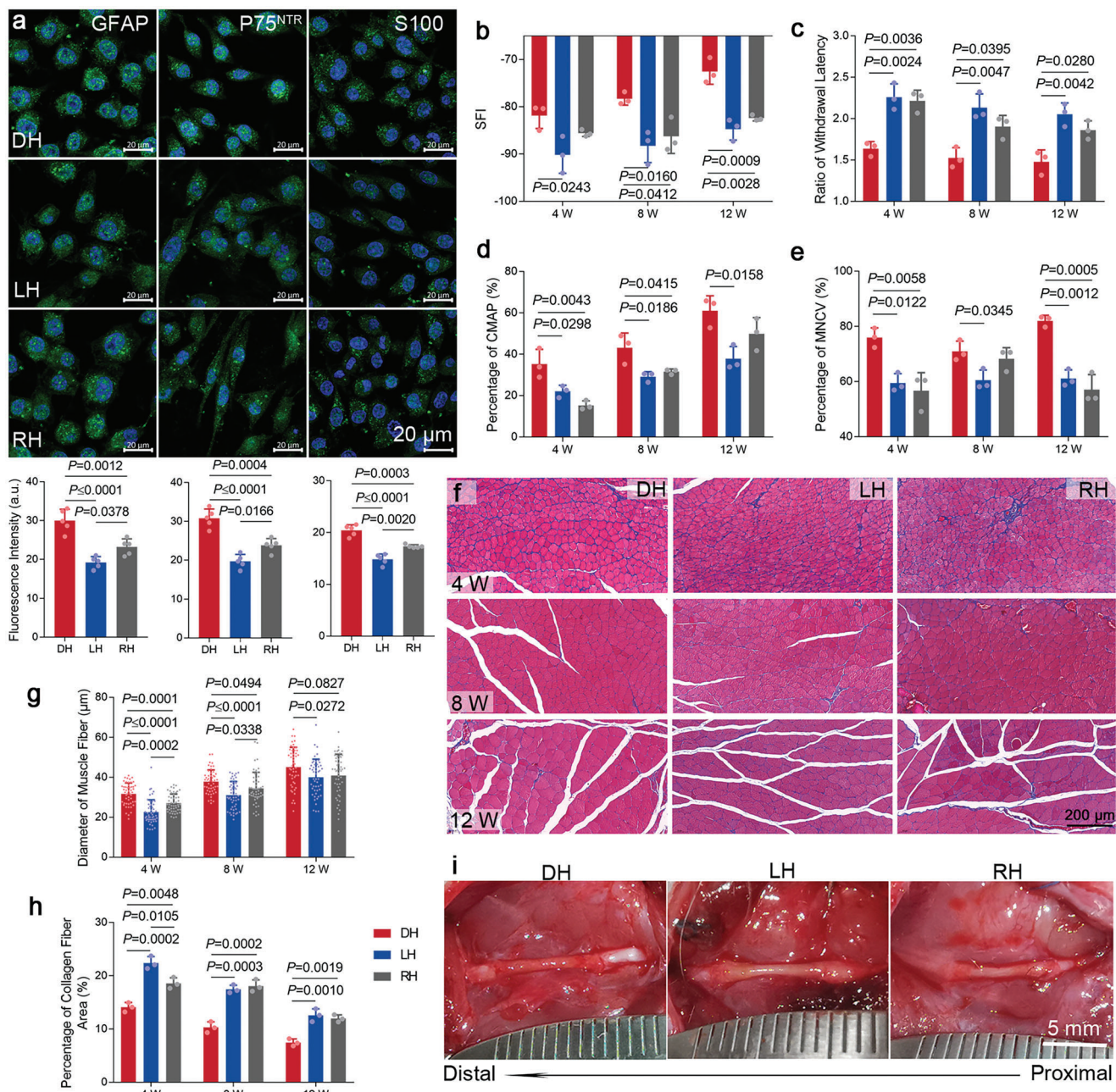


Figure 6. Functional recovery and physiological reconstruction in sciatic-nerve-deficient rats repaired using chiral matrixes. **a)** Representative images of IF-stained proteins involved in neurological functions in RSC96 cells cultured on chiral matrixes, along with the corresponding statistics of fluorescence intensity. Target proteins are shown in green, and DAPI-stained nuclei are shown in blue. **b–e)** SFI, ratio of withdrawal latency, and recovery percentage of CMAP, and MNCV in rats implanted with chiral matrixes at 4, 8, and 12 w postoperatively. **f–h)** Representative images of Masson-stained gastrocnemius muscles, along with quantification analyses of muscle fiber diameter and collagen fiber area percentage. **i)** Representative images of regenerated nerves at 12 w postoperatively. Values in (a–e), (g), and (h) represent the mean ± s.d. ($n = 5$ for (a), $n = 3$ for ((b)–(e) and (h)), and $n = 50$ for (g)). Statistical significance and P values were determined by one-way ANOVA followed by Tukey's multiple comparison test.

potential positive effect of D-matrix in peripheral nerve regeneration.

Therefore, rat sciatic nerve repair models were constructed with chiral matrixes implanted into the defects (Figure S13, Supporting Information). At 4, 8, and 12 w postoperatively, the functional recovery and electrophysiological reconstruction

were evaluated first. Based on walking track analyses, the highest sciatic function index (SFI) was observed in the DH group (Figure 6b), suggesting improved motor nerve function recovery by D-matrix implantation. A significant increase in the recovery ratio of hindfoot withdrawal latency for thermal stimulation was also observed in the DH group (Figure 6c), indicating

the best sensory nerve recovery by D-matrix implantation. Additionally, both recovery percentages of compound motor action potential (CMAP, Figure 6d) and motor nerve conduction velocity (MNCV, Figure 6e) were significantly improved in the DH group, demonstrating enhanced electrophysiological reconstruction by D-matrix implantation. Gastrocnemius muscles, the target organ of sciatic nerves, were processed with Masson-staining, and the cross-sectional area of muscle fibers was noticeably the largest in the DH group, with progressive growth from 4 to 12 w (Figure 6f). Statistically, in the DH group, the average diameter of muscle fibers was the largest (Figure 6g), and the percentage of collagen fiber area was the least (Figure 6h), suggesting maximal improvement of muscle atrophy following successful reinnervation. These results demonstrate that D-matrix chirality significantly improves functional recovery, electrophysiological reconstruction, and reinnervation of regenerated sciatic nerves.

Furthermore, all regenerated nerves were eumorphic without visible swelling, scarring, or inflammatory tissues (Figure 6i). Numerous regenerated microvessels in all groups (blue arrows) and trace amounts of residual hydrogel in a few images (black arrows) were observed (Figures S14 and S15, Supporting Information). These results suggest successful nerve regeneration without evident adverse effects in all experimental rats. Subsequently, IF staining was performed on nerve sections to label axons and Schwann cells with NF200 and S100, respectively. The DH group exhibited the strongest fluorescence intensity for both proteins, with more positive regions and larger aggregation spots (Figure 7a; Figure S16, Supporting Information), suggesting an improved Schwann cell population and facilitated axonal regeneration mediated by D-matrix chirality. Toluidine blue (TB)-stained nerve slices of the DH group exhibited distinctly larger myelinated nerve fibers from 4 to 12 w with multiple enormous fibers (black triangles) at 12 w (Figure 7b; Figure S17, Supporting Information), and TEM images showed the thickest myelin sheaths of nerve fibers in DH group (Figure 7c; Figure S18, Supporting Information). In statistics, although the density of nerve fibers in the DH group showed no advantage (Figure 7d), the myelinated nerves in the DH group had a significantly larger diameter (Figure 7e) and a higher percentage of axons with a diameter greater than 5 μm (Figure 7f; Figure S19, Supporting Information), indicating that numerous regenerated nerves in the DH group successfully reinnervated and continued to grow, while the others gradually degenerated.^[19] Meanwhile, the thickness of myelin sheaths remained the highest in the DH group from 4 to 12 w (Figure 7g). These results suggest that D-matrix chirality significantly promoted myelination and axonal growth of the regenerated nerves. Collectively, these findings demonstrate that D-chirality of the implanted matrix enhances sciatic nerve repair by improving the population, function, and myelination of Schwann cells and subsequently facilitating axonal regeneration and growth.

Considering the promising application of non-neural stem cells in various neurological therapies and the resulting contrast in matrix chirality selection, rat sciatic nerve repair models were again constructed with the implantation of chiral matrixes mixed with BMSCs. Under this condition, the DH group consistently showed improvements in function recovery (Figure S20a,b, Supporting Information), electrophysiological re-

construction (Figure S20c,d, Supporting Information), and reinnervation of gastrocnemius muscles (Figure S20e-g, Supporting Information) compared to the RH group, although the LH group showed the best recovery because of the highly significant efficacy of BMSCs reinforced by L-matrix chirality. With no visible swelling, scarring, or inflammatory tissue (Figures S20h, S21, and S22, Supporting Information), the IF-stained regenerated nerves (Figure S23, Supporting Information) exhibited stronger fluorescence intensity of NF200 and S100 labeling for axons and Schwann cells in the DH and LH groups, indicating an improved population of axons and Schwann cells. According to the statistical analyses of myelinated nerve fibers and myelin sheaths from nerve section images (Figures S24 and S25, Supporting Information), both DH and LH groups exhibited significantly larger average diameters of nerve fibers compared to the RH group at 4 w (Figure S26a,b, Supporting Information). However, the DH group had the significantly highest percentage of axons with a diameter greater than 5 μm (Figure S26c, Supporting Information), while the LH group showed higher nerve density (Figure S26d, Supporting Information). Moreover, the thickness of myelin sheaths in the DH group remained significantly the highest (Figure S26e, Supporting Information). These results indicate that L-matrix-reinforced BMSCs promote axon germination, while D-matrix promotes Schwann cell myelination. Overall, D-matrix consistently enhances sciatic nerve repair with transplanted BMSCs primarily by positively affecting Schwann cells, compared to the commonly used racemic matrix, despite the greater efficacy of L-matrix-reinforced BMSCs through directly encouraging axon regeneration.

3. Discussion and Conclusion

As a strict chiral system, living systems possess specific chirality selection at multiple levels from molecules to individuals.^[4] And with the presence of chiral recognition,^[20] we can manipulate cell behaviors by modifying the chirality of artificial extracellular matrixes. This study demonstrates the specific enhancement of the viability, proliferation, and survival of four neural cells by the D-matrix chirality (Figure 3; Figures S4–S6, Supporting Information), and we introduce chirality selection for the D-matrix as a new concept to define this potentially universal phenomenon in neural cells. We further propose the mechanism functioning through which the tension relaxation, resulting from weaker interaction between D-matrix and cytoskeleton, activates JNK and p38 MAPK signaling pathways (Figures 4 and 5; Figures S10–S12 and Tables S1–S5, Supporting Information).

This phenomenon observed in neural cells contrasts with the previously reported chirality selection for the L-matrix in various non-neuronal cells.^[6b–f,7a,c] However, it does not emerge without any indications. Organisms primarily utilize L-amino acids for protein synthesis, with negligible accumulation of D-amino acids in aging tissues.^[21] Nevertheless, D-serine and D-aspartate assume critical functions in the nervous system. D-serine, produced in neurons,^[22] is essential for neuronal death mechanisms^[23] and is involved in vital physiological and pathological processes, including learning and memory,^[24] synapse formation,^[25] epilepsy,^[26] and injury perception.^[27] Similarly, D-aspartate plays an important role in the nervous system and the neuroendocrine system, regulating the syntheses and release of several hormones

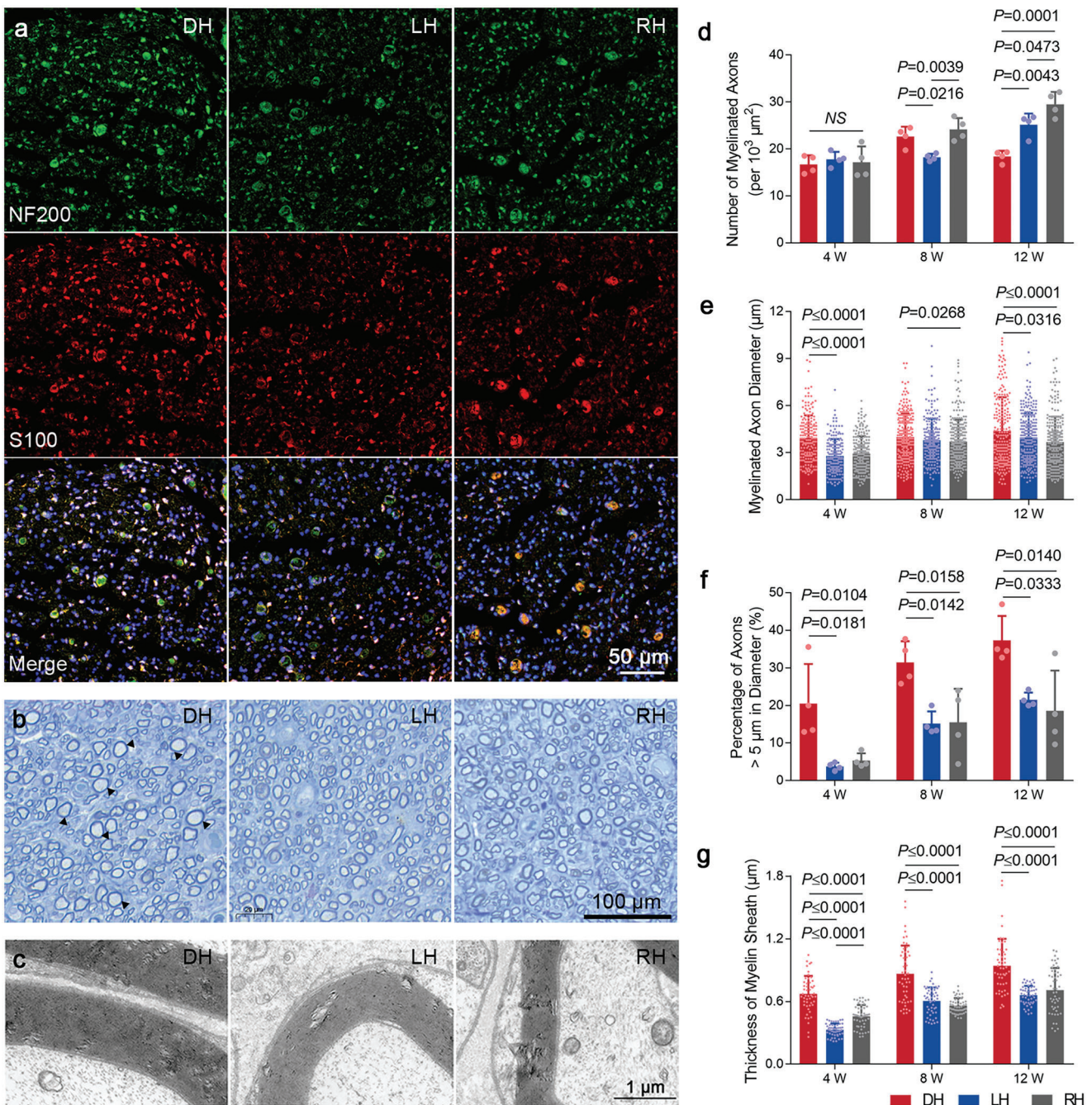


Figure 7. Evaluation of regenerated nerves in sciatic-nerve-deficient rats repaired using chiral matrixes. **a)** Representative images of nerve sections with IF-stained NF200 for axons and S100 for Schwann cells at 12 w postoperatively. DAPI-stained nuclei are shown in blue. **b)** Representative images of TB-stained nerve sections at 12 w postoperatively. Black triangles indicate enormous nerve fibers. **c)** Representative TEM images of myelin sheaths at 12 w postoperatively. **d–f)** Statistical analyses of myelinated nerve density, diameter, and percentage of myelinated axons with a diameter >5 μm , based on images of TB-stained regenerated nerves. **g)** Thickness of myelin sheaths according to TEM images of regenerated nerves. Values in **(d)–(g)** represent the mean \pm s.d. ($n = 4$ for **(d)** and **(f)**), $n = 256$ for **(e)**, and $n = 50$ for **(g)**). Statistical significance and P values were determined by one-way ANOVA followed by Tukey's multiple comparison test.

as well as the development of the nervous system.^[28] This discovery inspires us to consider the potentially extensive specificity of D-chirality in the nervous system and encourages further exploration into the chirality of molecules, proteins, and cells in the nervous system.

While rudimentarily relying on rat models, this study demonstrates that the application of D-matrix chirality alone can promote comprehensive repair of sciatic nerves with or without non-neuronal cell transplantation, including function recovery, electrophysiological reconstruction, and muscle reinnervation

(Figure 6; Figure S20, Supporting Information), achieved by enhancing axon growth and Schwann cell myelination (Figure 7; Figures S16–S19 and S23–S26, Supporting Information). Notably, the D-matrix selection of Schwann cells is deemed crucial, given the enhancements of injury activation (Figure 6a), proliferation, and survival of Schwann cells (Figure 3). Additionally, L-matrix also efficiently enhances sciatic nerve repair through reinforcing implanted BMSCs (Figure S8, Supporting Information). This study establishes the capability of matrix chirality as a novel and efficacious physicochemical cue to manipulate the behaviors of neural cells both in vitro and in vivo, which is safe, not extra immunogenic, and easy to perform. Prepared through suitable chiral material selection,^[8,29] polymer surface graft,^[20] or simple adsorption methods,^[30] chiral biomaterials are theoretically feasible and harmless to modulate the states and behaviors of neural cells, as well as altering the interaction between materials and different cells in vivo, holding extensive application potential in neurological issues such as central nerve regeneration, neurodegenerative disease treatment, neural tumor targeting, and neurodevelopment.

Naturally, this study has limitations and opens up multiple questions. It is only based on four kinds of neural cell lines and is not solid enough to reach a general principle applicable to all cells in the nervous system, whereas it is a good beginning to spark further research on the whole picture of chirality specificity in the nervous system. The natural extracellular matrix is a complex 3D network composed of multiple macromolecules, including collagens, glycosaminoglycans, elastin, fibronectin, laminins, and several glycoproteins,^[31] with no dominant chirality in its structure, although the major component is triple-helical right-handed collagens, which suggests that the matrix chirality serves as an external stimulus to the cells.

Overall, this study introduces matrix chirality as a previously unknown cue for specifically manipulating neural cell behaviors, particularly improving viability, proliferation, and survival. The molecular mechanism is that D-chirality attenuates interaction between matrixes and cytoskeleton, thus activating JNK and p38 MAPK signaling pathways. With the demonstrated promotion of sciatic nerve repair by D-chirality, we believe that matrix chirality is a simple, safe, and effective microenvironment cue with application potential in neurological issues such as nerve regeneration, neurodegenerative disease treatment, neural tumor targeting, and neurodevelopment.

Supporting Information

Supporting Information is available from the Wiley Online Library or from the author.

Acknowledgements

This work was supported by the National Natural Science Foundation of China (Nos. 52273139 and 52103177), the National Key Research and Development Program of China (No. 2018YFC1106800), Sichuan Science and Technology Program (Nos. 2023NSFSC0639 and 2023NSFSC1000), and CAS Key Laboratory of Bio-inspired Materials and Interfacial Science, Technical Institute of Physics and Chemistry. All animal experiments were in compliance with the principles for the care and use of laboratory animals and approved by the Animal Ethics Committee of Sichuan University (Approval No. KS2020039).

Note: The order in which the institutes appear in the affiliations was revised on September 7, 2023, after initial publication online.

Conflict of Interest

The authors declare no conflict of interest.

Author Contributions

Z.H., C.F., and Y.L. performed conceptualization. Y.L., Y.W., X.L., and N.M. performed methodology. Q.A., X.D., T.C., G.Y., X.P., J.W., and H.F. performed supervision. Y.L. performed visualization. Y.L. wrote original draft. Y.L., Z.H., C.F., and Q.A. wrote, reviewed, and edited the manuscript.

Data Availability Statement

The data that support the findings of this study are available in the supplementary material of this article.

Keywords

chiral materials, chirality selection, microenvironmental cues, nerve regeneration, neural cells, neurology

Received: February 14, 2023

Revised: June 16, 2023

Published online: July 23, 2023

- [1] N. Mitrousis, A. Fokina, M. S. Shoichet, *Nat. Rev. Mater.* **2018**, *3*, 441.
- [2] G. S. Hussey, J. L. Dziki, S. F. Badylak, *Nat. Rev. Mater.* **2018**, *3*, 159.
- [3] a) L. M. Y. Yu, N. D. Leipzig, M. S. Shoichet, *Mater. Today* **2008**, *11*, 36; b) Y. Li, Z. Huang, X. Pu, X. Chen, G. Yin, Y. Wang, D. Miao, J. Fan, J. Mu, *Colloids Surf. B* **2020**, *191*, 110972.
- [4] a) S. I. S. Hendrikse, R. Contreras-Montoya, A. V. Ellis, P. Thordarson, J. W. Steed, *Chem. Soc. Rev.* **2022**, *51*, 28; b) A. S. Chin, K. E. Worley, P. Ray, G. Kaur, J. Fan, L. Q. Wan, *Proc. Natl. Acad. Sci. USA* **2018**, *115*, 12188; c) M. Levin, *Mech. Dev.* **2005**, *122*, 3.
- [5] a) L. Xu, X. Wang, W. Wang, M. Sun, W. J. Choi, J.-Y. Kim, C. Hao, S. Li, A. Qu, M. Lu, X. Wu, F. M. Colombari, W. R. Gomes, A. L. Blanco, A. F. de Moura, X. Guo, H. Kuang, N. A. Kotov, C. Xu, *Nature* **2022**, *601*, 366; b) D. R. Griffin, M. M. Archang, C.-H. Kuan, W. M. Weaver, J. S. Weinstein, A. C. Feng, A. Ruccia, E. Sideris, V. Ragkousis, J. Koh, M. V. Plikus, D. Di Carlo, T. Segura, P. O. Scumpia, *Nat. Mater.* **2021**, *20*, 560; c) Y. Wei, S. Jiang, M. Si, X. Zhang, J. Liu, Z. Wang, C. Cao, J. Huang, H. Huang, L. Chen, S. Wang, C. Feng, X. Deng, L. Jiang, *Adv. Mater.* **2019**, *31*, 1900582; d) H. Zheng, T. Yoshitomi, K. Yoshimoto, *ACS Appl. Bio Mater.* **2018**, *1*, 538; e) E. Arslan, M. Hatip Koc, O. Uysal, B. Dikecoglu, A. E. Topal, R. Garifullin, A. D. Ozkan, A. Dana, D. Hermida-Merino, V. Castelletto, C. Edwards-Gayle, S. Baday, I. Hamley, A. B. Tekinay, M. O. Guler, *Biomacromolecules* **2017**, *18*, 3114; f) X. Yao, Y. Hu, B. Cao, R. Peng, J. Ding, *Biomaterials* **2013**, *34*, 9001.
- [6] a) K. Hou, J. Zhao, H. Wang, B. Li, K. Li, X. Shi, K. Wan, J. Ai, J. Lv, D. Wang, Q. Huang, H. Wang, Q. Cao, S. Liu, Z. Tang, *Nat. Commun.* **2020**, *11*, 4790; b) X. Zhao, L. Xu, M. Sun, W. Ma, X. Wu, C. Xu, H. Kuang, *Nat. Commun.* **2017**, *8*, 2007; c) T. Sun, D. Han, K. Rhemann, L. Chi, H. Fuchs, *J. Am. Chem. Soc.* **2007**, *129*, 1496; d) F. Zhou, L. Yuan, D. Li, H. Huang, T. Sun, H. Chen, *Colloids Surf. B* **2012**, *90*, 97; e) X. Wang, H. Gan, T. Sun, B. Su, H. Fuchs, D. Vestweber, S. Butz, *Soft Matter* **2010**, *6*, 3851; f) X. Wang, H. Gan, M. Zhang, T. Sun, *Langmuir* **2012**, *28*, 2791.

- [7] a) G. Liu, D. Zhang, C. Feng, *Angew. Chem., Int. Ed.* **2014**, *53*, 7789; b) A. Motealleh, H. Hermes, J. Jose, N. S. Kehr, *Nanomedicine: NBM* **2018**, *14*, 247; c) J. Liu, F. Yuan, X. Ma, D.-i. Y. Auphedeous, C. Zhao, C. Liu, C. Shen, C. Feng, *Angew. Chem., Int. Ed.* **2018**, *57*, 6475.
- [8] X. Dou, C. Feng, *Adv. Mater.* **2017**, *29*, 1604062.
- [9] a) K. Baranes, H. Moshe, N. Alon, S. Schwartz, O. Shefi, *ACS Chem. Neurosci.* **2014**, *5*, 370; b) N. Sun, X. Dou, Z. Tang, D. Zhang, N. Ni, J. Wang, H. Gao, Y. Ju, X. Dai, C. Zhao, P. Gu, J. Ji, C. Feng, *Bioact. Mater.* **2021**, *6*, 990; c) N. Sun, J. Wang, X. Dou, Y. Wang, Y. Yang, D. Xiao, P. Zhao, J. Li, S. Wang, P. Gu, J. Ji, *Biomater. Sci.* **2022**, *10*, 5938.
- [10] a) D. K. Smith, *Chem. Soc. Rev.* **2009**, *38*, 684; b) D. Yang, P. Duan, L. Zhang, M. Liu, *Nat. Commun.* **2017**, *8*, 15727.
- [11] a) G. Liu, D. Zhang, C. Feng, *Angew. Chem. Int. Ed. Engl.* **2014**, *53*, 7789; b) X. Dou, B. Wu, J. Liu, C. Zhao, M. Qin, Z. Wang, H. Schonherr, C. Feng, *ACS Appl. Mater. Interfaces* **2019**, *11*, 38568.
- [12] a) Y. Wang, Y. Li, Z. Huang, B. Yang, N. Mu, Z. Yang, M. Deng, X. Liao, G. Yin, Y. Nie, T. Chen, H. Ma, *Carbohydr. Polym.* **2022**, *290*, 119499; b) Y. Shi, X. Guo, J. Zhang, H. Zhou, B. Sun, J. Feng, *Brain, Behav. Immun.* **2018**, *73*, 482; c) D. Vaudry, P. J. S. Stork, P. Lazarovici, L. E. Eiden, *Science* **2002**, *296*, 1648.
- [13] K. Yamamoto, H. Miura, M. Ishida, Y. Mii, N. Kinoshita, S. Takada, N. Ueno, S. Sawai, Y. Kondo, K. Aoki, *Nat. Commun.* **2021**, *12*, 7145.
- [14] a) E. K. Kim, E.-J. Choi, *Biochim. Biophys. Acta Mol. Basis Dis.* **2010**, *1802*, 396; b) Y. Sun, W. Liu, T. Liu, X. Feng, N. Yang, H. Zhou, *J. Recept. Sig. Transd.* **2015**, *35*, 600; c) L. E. Rameh, L. C. Cantley, *J. Biol. Chem.* **1999**, *274*, 8347; d) C. Widmann, S. Gibson, M. B. Jarpe, G. L. Johnson, *Physiol. Rev.* **1999**, *79*, 143.
- [15] a) H. Ryu, H. N. Lee, J. Ju, J.-B. Park, E. Oh, M. Z. Lin, J. Seong, *Sens. Actuators, B* **2022**, *369*, 132316; b) V. Sauzeau, I. M. Berenjeno, C. Citterio, X. R. Bustelo, *Oncogene* **2010**, *29*, 3781.
- [16] a) L. H. Easson, E. Stedman, *Biochem. J.* **1933**, *27*, 1257; b) R. Bentley, *Nature* **1978**, *276*, 673.
- [17] J. H. Sohn, C. H. Kim, S. H. Lee, J. H. Kim, J. J. Lee, *Front. Med.* **2020**, *7*, 84.
- [18] H. Hirata, H. Hibasami, T. Yoshida, M. Ogawa, M. Matsumoto, A. Morita, A. Uchida, *Glia* **2001**, *36*, 245.
- [19] a) X. Gu, F. Ding, D. F. Williams, *Biomaterials* **2014**, *35*, 6143; b) T. Gordon, *Int. J. Mol. Sci.* **2020**, *21*, 8652.
- [20] M. Zhang, G. Qing, T. Sun, *Chem. Soc. Rev.* **2012**, *41*, 1972.
- [21] S. Ritz-Timme, M. J. Collins, *Ageing Res. Rev.* **2002**, *1*, 43.
- [22] D. Rosenberg, E. Kartvelishvily, M. Shleper, C. M. Klinker, M. T. Bowser, H. Wolosker, *FASEB J.* **2010**, *24*, 2951.
- [23] M. Shleper, E. Kartvelishvily, H. Wolosker, *J. Neurosci.* **2005**, *25*, 9413.
- [24] G. Collingridge, *Nature* **1987**, *330*, 604.
- [25] W. Danysz, C. G. Parsons, *Pharmacol. Rev.* **1998**, *50*, 597.
- [26] L. Giraldez, E. Girardi, *Neurochem. Int.* **2000**, *36*, 243.
- [27] E. Palazzo, V. de Novellis, I. Marabese, D. Cuomo, F. Rossi, L. Berrino, F. Rossi, S. Maione, *Eur. J. Pharmacol.* **2002**, *439*, 69.
- [28] a) H. Wang, H. Wolosker, J. F. Morris, J. Pevsner, S. Snyder, D. Selkoe, *Neuroscience* **2002**, *109*, 1; b) A. D'Aniello, *Brain Res. Rev.* **2007**, *53*, 215; c) T. Furuchi, H. Homma, *Biol. Pharm. Bull.* **2005**, *28*, 1566.
- [29] R. M. Hazen, D. S. Sholl, *Nat. Mater.* **2003**, *2*, 367.
- [30] R. Raval, *Chem. Soc. Rev.* **2009**, *38*, 707.
- [31] A. D. Theocaris, S. S. Skandalis, C. Gialeli, N. K. Karamanos, *Adv. Drug Delivery Rev.* **2016**, *97*, 4.
- [32] J. R. Bain, S. E. Mackinnon, D. A. Hunter, *Plast. Reconstr. Surg.* **1989**, *83*, 129.
- [33] a) W. D. Arnold, K. A. Sheth, C. G. Wier, J. T. Kissel, A. H. Burghes, S. J. Kolb, *J. Vis. Exp.* **2015**, *25*, e52899; b) E. Pollari, R. Prior, W. Robberecht, P. Van Damme, L. Van Den Bosch, *J. Vis. Exp.* **2018**, *15*, e57741.